A Bayesian Approach to Fused GRAPPA and SENSE MR Image Reconstruction

Chase J. Sakitis [a], Daniel B. Rowe [a]

[a] *Department of Mathematical and Statistical Sciences, Marquette University, Milwaukee Wisconsin, USA*

Abstract

In fMRI, capturing brain activity during a physical task is dependent on how quickly each volume *k*-space array is obtained. Acquiring the full *k*-space arrays can take a considerable amount of time. Under-sampling *k*-space reduces the acquisition time, but results in aliased, or "folded", images after applying the inverse Fourier transform (IFT). GeneRalized Autocalibrating Partial Parallel Acquisition (GRAPPA) and SENSitivity Encoding (SENSE) are parallel imaging techniques that yield full images from subsampled arrays of *k*-space. With GRAPPA operating in the spatial frequency domain and SENSE in image space, these techniques can be fused to reconstruct the subsampled *k*-space arrays more accurately. Here, we propose a Bayesian approach to this combined model where prior distributions for the unknown parameters are assessed from *a priori k*-space arrays. The prior information is utilized to estimate the missing spatial frequency values, unalias the voxel values from the posterior distribution, and reconstruct into full field-of-view images. Our Bayesian technique successfully reconstructed a simulated fMRI time series with no aliasing artifacts while decreasing temporal variation.

Key Words: Bayesian, GRAPPA, fMRI, reconstruction, SENSE

1. Introduction

1.1 Background

Functional Magnetic Resonance Imaging (fMRI) is a medical imaging technique that was developed in the early 1990's as a technique to noninvasively observe human brain activity without exogenous contrast agents [2]. When a neuron fires, changes in the blood oxygenation using the blood oxygen-level dependent (BOLD) contrast is detected in its proximity [14] which can be used to map brain activity [15]. The magnetic resonance imaging (MRI) scanner measures arrays of complex-valued spatial frequencies called *k*-space [9]. These *k*-space arrays are then transformed into brain images using an inverse Fourier transform (IFT). The reconstructed brain images are made up of complex-valued voxels which contain the signal intensity (magnitude) and a measure of local magnetic field (phase) for each pixel in the image.

For fMRI analysis, the phase images are typically discarded. For this research, phase images will be utilized for reconstruction analysis. Producing magnitude and phase images is simply a conversion to polar coordinates from Cartesian coordinates in the complex plane. The concentration here will be on Cartesian *k*-space sampling with the conversion to polar coordinates used for reconstruction analysis and image depiction purposes.

In fMRI, obtaining hundreds of volume images is necessary to statistically detect activation. This series of images is the same underlying volume image measured individually through time. It takes a considerable amount of time to measuring full *k*-space arrays for all slices required to form volume images due to the size of a dataset from a single experiment. This lengthy acquisition time limits the temporal resolution of the reconstructed images which can diminish the ability to capture brain activity. A key focus in recent MR research has been reducing the scan time of the fMRI process has been by accelerating the number of images acquired per unit of time [6, 7, 16].

1.2 Previous Approach

The introduction of parallel imaging techniques allow more images per unit of time to be acquired by measuring less data without losing the ability to form a full field-of-view (FOV) reconstructed image. With these techniques, multi-channel receiver coils are utilized in parallel to fully sample *k*-space data arrays instead of using the historically used single channel receiver coil. Utilization of multiple receiver coils allows researchers to skip lines of the *k*-space arrays during the acquisition process. This yields subsampled spatial frequency arrays for each coil and reduces the acquisition time of the *k*-space arrays. However, skipping lines in *k*-space causes the images in each coil, after using the IFT, to be aliased, or appear "folded over." To produce a single, full FOV, reconstructed brain image, the multiple aliased coil images are required to be unaliased and combined.

There are two common parallel imaging techniques that accomplish this: GeneRalized Autocalibrating Partial Parallel Acquisition (GRAPPA) [6] and SENSitivity Encoding (SENSE) [16]. GRAPPA operates on the subsampled *k*-space prior to the IFT by assessing localized weights that are used to interpolate the unacquired spatial frequencies for each coil. SENSE operates in image space after the IFT utilizing estimated coil sensitivities (coil weightings) to unalias and combine the aliased coil measurements into a single FOV image.

For the GRAPPA method, once the unacquired spatial frequencies are interpolated, the full coil spatial frequency arrays (acquired plus estimated) are combined into a single *k*-space array by averaging the coil spatial frequency values at each location. The IFT is applied to the averaged, full *k*-space array to transform the spatial frequency array into a brain image. GRAPPA is effective with low acceleration factors since it does not rely on sensitivity coil information but has its deficiencies at higher acceleration factors. These deficiencies include low image quality, low SNR, and diminished task detection power [4]. We developed a Bayesian approach to GRAPPA (BGRAPPA) that incorporates more prior information to estimate the unacquired spatial frequencies [20]. BGRAPPA increased SNR and image quality and displayed improved power in detecting task compared to GRAPPA.

The SENSE method uses complex-valued linear regression with a fixed design matrix on the aliased coil measurements after the IFT. SENSE then uses a least squares solution to estimate the voxel values of the single, reconstructed brain image, but this can be difficult because the complex-valued design matrix can be ill-conditioned. This parameter estimation approach can cause low image quality, aliasing artifacts, and signal-to-noise ratio (SNR) degradation in the final reconstructed image. These deficiencies have led to variations of the traditional technique [8, 10, 11, 12], but hardly mitigate the limitations of the traditional maximum likelihood SENSE procedure. We have previously developed a Bayesian approach to SENSE (BSENSE) that incorporates more prior information in the estimated voxel values of the full FOV reconstructed image [19]. When comparing BSENSE to SENSE, the results yielded no aliasing artifacts with increased SNR, image quality, and task detection power [19].

Here, we first introduce a merged utilization of GRAPPA and SENSE (MUGS) for in-plane accelerated image reconstruction. This technique is a two-step reconstruction process. First, GRAPPA is utilized to estimate the unacquired spatial frequencies yielding full coil *k*-space arrays. Using the IFT, these full coil *k*-space arrays are reconstructed into coil-weighted brain images. The second step uses SENSE to combine the coil-weighted images into a single, complex-valued brain image. This MUGS technique utilizes information from both the spatial frequency domain and the image space domain to reconstruct the subsampled coil *k*-space arrays into a single full FOV brain image. Despite this merged utilization of both traditional reconstruction techniques, it does not take advantage of all valuable available prior information that can be incorporated into the reconstructed image. Here, we propose a Bayesian approach to MUGS (BMUGS) that instead of merging GRAPPA and SENSE, we merge BGRAPPA and BSENSE. An fMRI simulation study is performed illustrating how the BMUGS technique outperforms the MUGS technique.

2. BMUGS Technique

2.1 Research Problem

From a single channel coil, full spatial frequency arrays are acquired along a trajectory, as shown in Figure 1 (left), following a Cartesian path with turnaround points at the end of each row. With acquiring full complex-valued spatial frequency arrays from a single channel coil, one only needs to use the IFT to yield a full FOV complex-valued brain image. Since the objective of this research is to acquire more images per unit of time, parallel imaging is utilized. This allows for subsampling of *k*-space. The right of Figure 1 shows the trajectory for undersampling the spatial frequencies. Like the fully sampled *k*-space array on the left side of Figure 1, the scanner starts in the bottom left and moves across the row acquiring complex-valued spatial frequency points along the row. Then, at the end of the row, it skips lines according to the acceleration factor n_A as it moves up the rows. We see that in Figure 1 (right), the trajectory skips the next one line, with an acceleration factor of $n_A = 2$, acquiring the second line above the bottom. This acquisition process is repeated until all designated rows of the discretized subsampled *k*-space array are acquired.

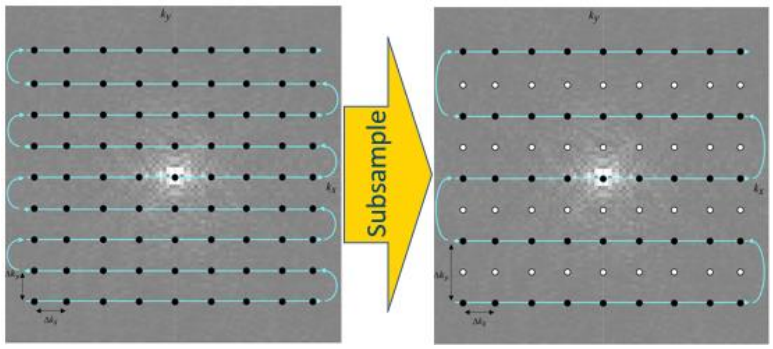

Figure 1: Trajectories of a fully sampled *k*-space array (left) and a subsampled *k*-space array with an acceleration factor of $n_A = 2$ (right).

To appropriately subsample the *k*-space arrays, $n_C > 1$ receiver coils are utilized in parallel instead of a single channel coil. For example, if there was a four-channel coil alignment, it can be arranged with the first coil located at the anterior and rotated clockwise around a subjects head when

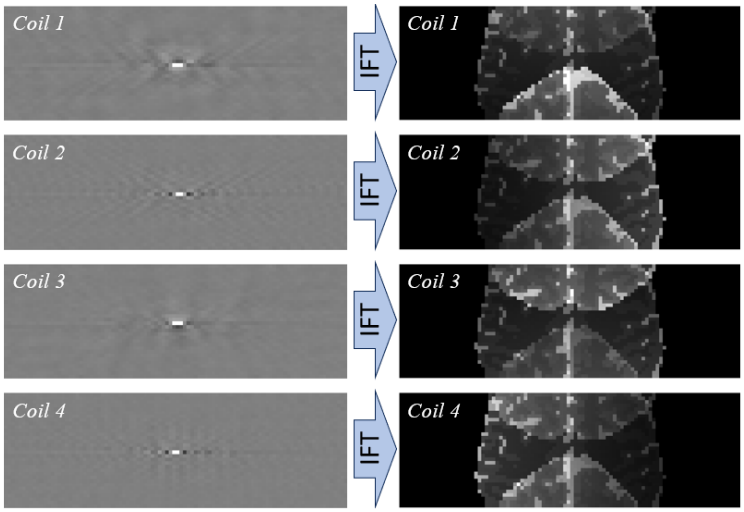

Figure 2: Illustration of $n_C = 4$ subsampled coil *k*-space arrays with an acceleration factor of $n_A = 3$ (left) and their respective aliased brain images after the IFT (right).

looking from the top of the head. With $n_A = 3$, each of the $n_C = 4$ coils acquire subsampled *k*-space as depicted on the left side of Figure 2. Then, using the IFT yields aliased brain images for each coil as shown on the right side of Figure 2. Due to the aliasing, these coil brain images are rendered useless as there is no distinct anatomical structure which makes it difficult to perform any fMRI analysis. Since these aliased images cannot be used, parallel imaging techniques are required to unfold and combine them into a single composite brain image.

2.2 Reconstruction Process

As previously mentioned, multiple steps are required to properly merge GRAPPA and SENSE together for in-plane accelerated image reconstruction. The process for reconstructing subsampled coil *k*-space arrays into a single brain image using the MUGS (and BMUGS) technique is demonstrated in Figure 3. In step 1 of Figure 3, pre-scan calibration spatial frequency arrays are acquired and utilized for estimating the localized weights, W_c, for GRAPPA in step 2. Also from step 1, the full coil spatial frequency arrays are transformed using the IFT to full coil-weighted brain images that are utilized to assess the coil sensitivities, *S*, for SENSE (step 2). Step 3 is then to acquire the subsampled spatial frequency arrays for the fMRI experiment. In step 4, GRAPPA is utilized to estimate all the unacquired spatial frequencies yielding full coil *k*-space arrays. These full coil *k*-space arrays are then transformed to coil-weighted images (step 5). Then SENSE reconstruction uses the pre-assessed coil sensitivity information to combine the coil images into a single composite brain image in step 6. This process is repeated for each time point in the subsampled fMRI time series. For the BMUGS technique, it follows the same procedure as the MUGS technique, but instead of GRAPPA and SENSE, BGRAPPA and BSENSE are applied respectively.

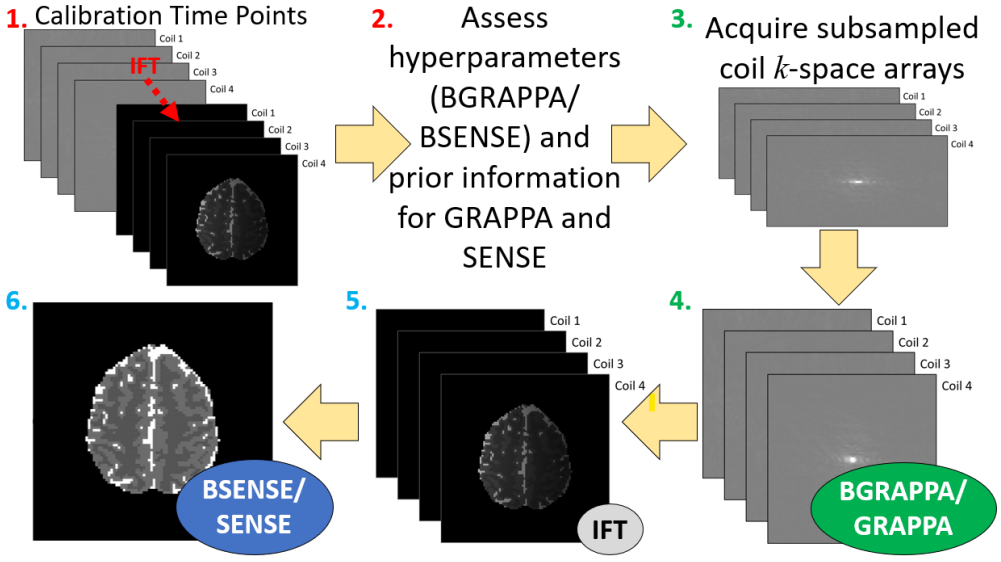

Figure 3: Flow chart for the BMUGS and MUGS model for image reconstruction.

The model for MUGS begins with the GRAPPA model. That is

$$f_{ec}^{(\omega)} = W_c^{(\omega)} f_{kc}^{(\omega)} + \eta_c^{(\omega)}, \qquad [2.1]$$

where $\omega = 1, \ldots, K$, $f_{ec} \in \mathbb{C}^{n_C \times 1}$ represents the complex-valued interpolated *k*-space values, $f_{kc} \in \mathbb{C}^{p \times 1}$ represents the complex-valued acquired *k*-space values, $\eta_c \in \mathbb{C}^{n_C \times 1}$ represents the additive complex-valued noise with $\eta_c \sim N(0, \tau^2(1+i))$, and $p = n_C k_{rows} k_{cols}$ and $K = n_y n_x (1 - 1/n_A)$, where n_y and n_x are the number of rows and columns, respectively, in the reconstructed image. For the BGRAPPA component of the BMUGS technique, the same linear model expressed in Eq. 2.1 is utilized, but the assignment of the parameters are different compared to MUGS. For BGRAPPA, $f_{ec} \in n_C \times 1$ represents the complex-valued acquired *k*-space values and $f_{kc} \in \mathbb{C}^{p \times 1}$ represents the complex-valued interpolated *k*-space values. This allows for the f_{kc}, W_c, and τ^2 parameters to be

treated as unknowns and place prior distributions on them. The interpolated spatial frequencies, f_{ec} for GRAPPA and f_{kc} for BGRAPPA, are then imputed in the respective locations of the missing *k*-space values resulting in full coil *k*-space arrays, f_{full}.

The full coil *k*-space arrays f_{full} are then inverse Fourier transformed into coil images. The SENSE model is then employed to combine the full FOV coil image measurements to obtain a single composite brain image. The model for SENSE is

$$a_c^{(\delta)} = S_c^{(\delta)} v_c^{(\delta)} + \varepsilon_c^{(\delta)} \quad [2.2]$$

where $\delta = 1, ..., M$, $a_c \in \mathbb{C}^{n_C \times 1}$ represents the complex-valued coil measurements, $S_c \in \mathbb{C}^{n_C \times 1}$ represents the matrix of complex-valued coil sensitivities, $v_c \in \mathbb{C}$ represents the complex-valued unaliased voxel value, $\varepsilon_c \in \mathbb{C}^{n_C \times 1}$ represents the additive complex-valued noise where $\varepsilon_c \sim N(0, \sigma^2 (1+i))$, and $M = n_y n_x$. For the BSENSE component of the BMUGS technique, the same linear model expressed in Eq. 2.2 is used. For BSENSE, the S_c, v_c, and σ^2 parameters are treated as unknowns with prior distributions. The BGRAPPA and BSENSE reconstruction techniques are detailed in the [20] and [19] papers.

3. Simulation Study

3.1 Spatial Frequency Data

A noiseless non-task image was used to create a series of 510 simulated full coil images for one slice that was utilized for pre-scan calibration assessment (step 1 in Figure 3). A noiseless task image was also used along with the noiseless non-task image was used to generate a separate series of 510 simulated full coil images for one slice mimicking real-world fMRI data. The region of interest (ROI) for the simulated task activation was derived from an fMRI experiment in which the subject tapped their right fingers leading to activity in the left motor cortex. With this knowledge, artificial magnitude intensity and phase angle signal increase was added to the voxels in the ROI. These two data sets were used for testing and comparing BMUGS and MUGS.

For the simulated experiment, the last $n_{cal} = 30$ time points of the non-task time series served as the calibration information utilized for prior information for MUGS (i.e. estimating the localized weights for the GRAPPA component and coil sensitivities for the SENSE component) and hyperparameter assessment for BMUGS. The second series, containing both non-task and task time points, was used for simulating a subsampled real-world fMRI experiment. The complex-valued images in both series were multiplied by a designed sensitivity map with $n_C = 8$ coils. In real-world MRI experiments, magnetization takes a few seconds to stabilize, leading to the first few images having increased signal compared to the rest of the series. To replicate this increased signal, the first three images in both time series are appropriately scaled based on experimental data. Both series were then Fourier transformed into full coil *k*-space arrays. These series were simulated by adding $N(0, 0.0036 n_y n_x)$ spatial noise, where n_y and n_x are the number of rows and columns, respectively, to the real and imaginary parts of the full coil *k*-space arrays, corresponding to the noise in real-world fMRI experimental data. The series of $n_{cal} = 30$ non-task time points were utilized to assess prior information for the BGRAPPA component and GRAPPA component of BMUGS and MUGS, respectively, while still in the spatial frequency domain. This non-task series was then inverse Fourier transformed into the image domain to assess the prior information for BSENSE and SENSE components of BMUGS and MUGS, respectively. The series of images for the fMRI simulated experiment were Fourier transformed into full coil *k*-space arrays. To mimic the fMRI experiment, the first 20 time points of the fMRI time series were discarded leaving 490 time points of spatial frequency arrays for the single slice. The remaining 490 time points in the time series were subsampled by censoring lines in *k*-space according to an acceleration factor of $n_A = 3$, leaving a series of 490 time points with an 8-channel coil of 32×96 subsampled arrays to be reconstructed by BMUGS and MUGS.

3.2 Reconstruction Results

To analyze the reconstruction performance of BMUGS vs. MUGS, we first evaluate the first time point of the reconstructed subsampled coil spatial frequencies. The magnitude (first row) and the phase (second row) of the true simulated image (first column), the BMUGS reconstructed image (second column), and MUGS reconstructed image (third column) are displayed in Figure 4.

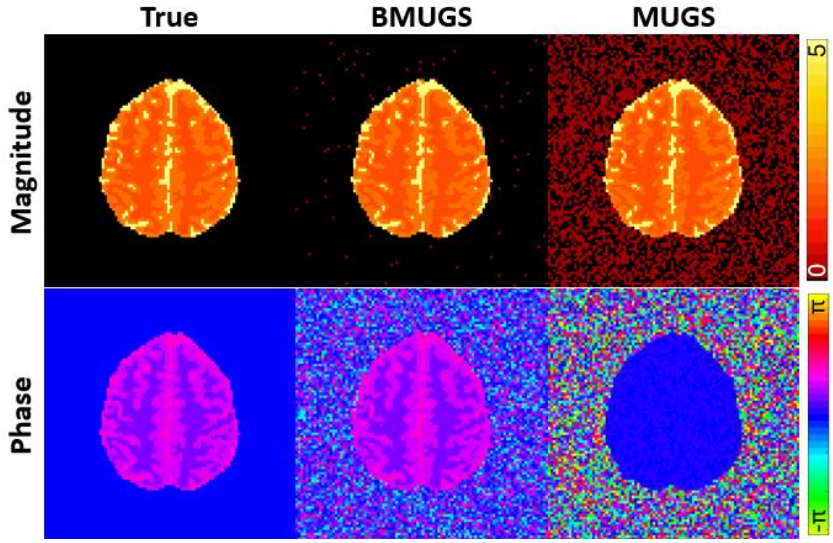

Figure 4: Magnitude (top row) and phase (bottom row) of the BMUGS (second column) and MUGS (third column) reconstructed images compared to the true simulated images (first column).

Analyzing Figure 6, we see that the BMUGS and MUGS magnitude images both closely resemble the true magnitude image inside the brain with the MUGS magnitude image being slightly noisier. This is more evident when looking outside the brain as the noise level is noticeably higher for MUGS compared the BMUGS which has little noise outside the brain. When looking at the phase images, BMUGS produces a better phase image as the MUGS phase image shows no anatomical structure.

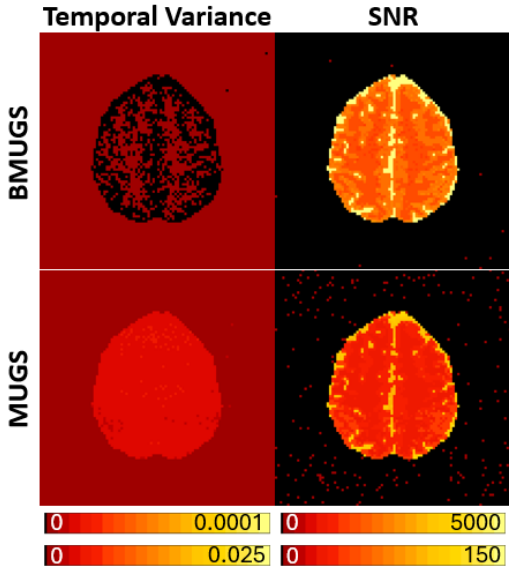

Figure 5: Temporal variance (first column) and SNR (second column) for BMUGS (first row) and MUGS (second row).

Next, we analyzed the entire reconstructed time series instead of just the first time point. Figure 5 shows the temporal variance of the time series for both techniques along with the signal-to-noise ratio (SNR) value of each reconstructed voxel. For both columns, there are two separate scales where the top scale is for the BMUGS technique, and the bottom scale is for the MUGS technique. Examining the temporal variance column, we see that BMUGS has a remarkably lower temporal variance which indicates that BMUGS reconstructed images are more accurate through time. Temporal variance also has a direct relationship with SNR which is why BMUGS has prominently higher SNR values compared to MUGS as shown in the second column of Figure 5. A larger SNR value indicates that the reconstruction technique is less affected by noise further showing the accuracy of the BMUGS reconstruction technique compared to MUGS.

After evaluating non-task results above, we next examined the task detection results since the primary goal of fMRI is to analyze brain activity. The left column of Figure 6 displays the results of task detection for BMUGS and MUGS, with the ROI outlined in green, using 5% false discovery rate (FDR) threshold procedure [3, 5], which generated a threshold of 3.82, with a closer view in the right column of the figure. When evaluating the task detection results in Figure 6, we can see that BMUGS captures the majority of the active voxels in our ROI whereas MUGS only captures four voxels indicating that BMUGS has a stronger power of task detection. The average *t*-statistic for BMUGS further supports this conclusion as it is markedly higher than the *t*-statistic for MUGS.

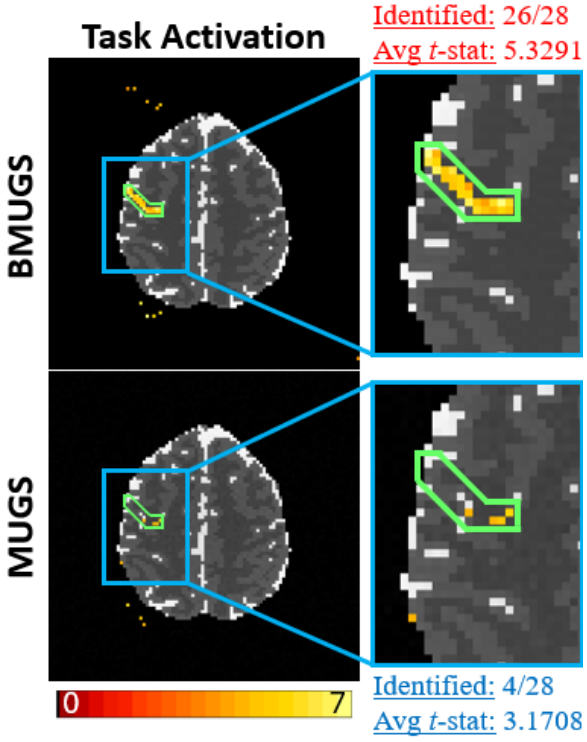

Figure 6: Task detection results (left column) for BMUGS (first row) and MUGS (second row) with a zoomed in view of the ROI and *t*-statistic analysis (right column) for both techniques.

4. Discussion

In this research, we formulated an image reconstruction technique that merges GRAPPA and SENSE (MUGS) for in-plane accelerated subsampled fMRI experiment. We then followed a Bayesian approach to MUGS parallel fMRI image reconstruction to incorporate all available calibration image information from the spatial frequency domain and image domain into the reconstruction process. Our proposed BMUGS method treats the unacquired spatial frequencies, the localized weights, the *k*-space noise variance, unaliased voxel values, coil sensitivities, and the image noise variance as unknowns and placed prior distributions on these parameters. Both techniques were tested and compared through a simulation study that mimics an experimental fMRI

study. The simulated results indicated a more accurate reconstructed image, a decreased temporal variance, higher SNR, and exceptional stronger power of task detection with BMUGS.

For the task activation results, a magnitude-only activation model was utilized which ignores the phase component of the complex-valued reconstruction time series. Despite the phase information being largely unused in fMRI studies, there is valuable information that can be extracted from the phase images [1]. The phase information can be utilized for task detection purposes using a phase-only task activation model [16]. Also, since the reconstructed images are complex-valued, our Bayesian model is applicable for complex activation models for task detection [16, 17].

The next steps for this work are to test different number of calibration time points used for hyperparameter assessment and applying different acceleration factors. More work with the simulation study will also include analysis of correlation between voxels and the voxels they were previously aliased with. After exhaustive testing using the simulated data sets, BMUGS and MUGS will be applied to experimental fMRI data with comparisons. The simulation and experimental studies performed for this paper are both in fMRI analysis, but this methodology can also be applied to diffusion weighted imaging [13].

References

1. Adrian, D. W., Maitra, R., and Rowe, D. B., *Complex-valued time series modeling for improved activation detection in fMRI studies*. Ann. Of Appl. Stat. 12 (3), 1451-1478, 2018.
2. Bandettini P, Jesmanowicz A, Wong E, Hyde J., *Processing strategies for time-course data sets in functional MRI of the human brain.* Mag. Res. Med 30 (2), 161–173, 1993.
3. Benjamini, Y., Hochberg, Y., *Controlling the false discovery rate: a practical and powerful approach to multiple testing*. J. R. Stat. Soc. B, 57 (1), 289 – 300, 1995.
4. Deshmane, A., Gulani, V., Griswold, M. A., and Seiberlich, N., *Parallel MR imaging*. Magnetic Resonance Imaging, 36 (1), 55-72, 2012.
5. Genovese, C. R., Lazar, N. A., and Nichols, T. E., *Thresholding of statistical maps in functional neuroimaging using the false discovery rate*. NeuroImage, 15 (4), 870-878, 2002.
6. Griswold MA, Jamob PM, Heidemann RM, Nittka M, Jellus V, Wang J, Kiefer B, Haase A., *Generalized autocalibrating partially parallel acquisition* (*GRAPPA*). Mag. Res. Med, 47 (6), 1202–1210, 2002.
7. Hyde JS, Jesmanowicz A, Froncisz W, Kneeland JB, Grist TM, Campagna NF. *Parallel image acquisition from noninteracting local coils.* J. Mag. Res, 70 (3), 512–517, 1986.
8. King, K. F., and Angelos, L., *SENSE image quality improvement using matrix regularization*. Proc. of the 9th Ann. Meet. of ISMRM, 1771, 2001.
9. Kumar, A., Welti, D., and Ernst, R. R., *NMR Fourier zeugmatography*. J. Mag. Res., 18 (1), 69-83, 1975.
10. Liang, Z. P., Bammer, R., Ji, J., Pelc, N. J., and Glover, G. H., *Making better SENSE: wavelet denoising, Tikhonov regularization, and total least squares*. Proc. of the 10th Ann. Meet. of ISMRM, 2388, 2002.
11. Lin, F. H., Kwong, K. K., Belliveau, J. W., and Wald, L. L., *Parallel imaging reconstruction using automatic regularization*. Mag. Res. Med., 51 (3), 559-567, 2004.
12. Liu, B., King, K., Steckner, M., Xie, J., Sheng, J., and Ying, L., *Regularized sensitivity encoding* (*SENSE*) *reconstruction using Bregman iterations*. Mag. Res. Med., 61 (1), 145-152, 2009.
13. Moon, W. J., Lee, M. H., and Chung, E. C., *Diffusion-weighted imaging with sensitivity encoding* (*SENSE*) *for detecting cranial bone marrow metastases: comparison with T1-weighted images*. Korean Journal of Radiology, 8 (3), 185-191, 2007.
14. Ogawa S, Lee TM, Nayak AS, Glynn P. *Oxygenation-sensitive contrast in magnetic resonance image of rodent brain at high magnetic fields.* Mag. Res. Med 14 (1), 68–78, 1990.
15. Ogawa, S., Tank, D. W., Ravi, M., Ellermann, J. M., Kim, S. G., Merkle, H., and Ugurbil, K., *Intrinsic signal changes accompanying sensory stimulation: Functional brain mapping with magnetic resonance imaging*. Proc. of the Nat. Acad. of Sci. USA, 89 (13), 5951-5955, 1992.
16. Pruessmann KP, Weiger M, Scheidegger MB, Boesiger P. *SENSE: Sensitivity Encoding for Fast MRI.* Mag. Res. Med, 42 (5), 952–962, 1999.

17. D. B. Rowe, *Modeling both the magnitude and phase of complex-valued fMRI data*. Neuroimage 25 (4), 1310–1324, 2005.
18. D. B. Rowe, B. R. Logan, *A complex way to compute fMRI activation*. Neuroimage 23 (3), 1078–1092, 2004.
19. Sakitis, C. J., Brown, D. A., and Rowe, D. B., *A Bayesian complex-valued latent variable model applied to functional magnetic resonance imaging*. J. R. Stat. Soc. C, qlae046, 2024.
20. Sakitis, C. J., and Rowe, D. B., *A Bayesian approach to GRAPPA parallel fMRI image reconstruction increases SNR and power of task detection*. Ann. of Appl. Stat., In Press, 2024.